O.M. Popovych, I. M. Budzulyak, O.V. Popovych, B.I. Rachiy, R.V. Ilnytskyi,
L.S. Yablon, O.V. Morushko

Synthesis and Electrochemical Properties of Nanocrystalline Nickel Molybdate

Vasyl Stefanyk Precarpathian National University, Ivano-Frankivsk, Ukraine, khemiiolha@gmail.com

We have obtained nanocrystalline hydrate and alpha phase of nickel molybdate by a hydrothermal technique. On the basis of the obtained cyclic voltammetry data, we have evaluated the contribution of faradaic and non-faradaic processes to the total capacitance of molybdates under study. It was found that the specific capacitance of hydrate $NiMoO_4 \cdot H_2O$ is 621 F/g at a scan rate of 1 mV / s and the specific capacitance of the α-$NiMoO_4$ is 281 F/g. Cathodes for hybrid supercapacitors were formed on the basis of the obtained nickel molybdates. As a result of electrochemical studies, it was found that the specific capacitance of hybrid supercapacitor based on $NiMoO_4 \cdot H_2O/C$ was 256 F/g at the current of 0.2 A/g, while the specific energy was 80 W h/kg and specific power – 304 W/kg and these results are higher below in the α-$NiMoO_4$ /C-based hybrid supercapacitor.

Keywords: nickel molybdate, hydrate, cyclic voltammogram, specific capacitance, coulombic efficiency, activated carbon, hybrid supercapacitor.

Introduction

Among the binary metal oxides used as electrodes in energy-storage devices, nanocrystalline nickel molybdate ($NiMoO_4$) is competitive due to its high electrochemical activity resulting from the reversible redox Ni^{2+} / Ni^{3+} reaction [1] and the crystal structure of the spinel type, which can provide efficient charge storage and high ion diffusion rate due to its three-dimensional network [2]. There are two polymorphic modifications of nickel molybdate under atmospheric pressure: α-$NiMoO_4$ (phase at low temperature) and β-$NiMoO_4$ (phase at high temperature) and molybdate may exist as a hydrate $NiMoO_4 \cdot H_2O$ [3]. The phases crystallized in the monoclinic crystal structure. The most obvious difference between the α and β phase is the coordination of Mo^{+6} ions which is octahedral in α-$NiMoO_4$ and tetrahedral in β-$NiMoO_4$. The α phase can be converted to the β phase when heated to temperature of 650 ºC, which is unstable and turns into the α phase when the temperature decreases [4]. It is known [5] that the hydrated structure of molybdate can provide better

electrochemical parameters compared to the pure phase due to low crystallinity and higher specific surface area. However, the poor electrical conductivity of $NiMoO_4$ slows down the electron / ion transfer process during charge / discharge and ultimately affects the specific capacitance of the material. In addition, large changes in volume during multiple cycling lead to degradation of the $NiMoO_4$ structure and consequently degrades the electrochemical performance of the material. Various approaches are implemented to increase the specific energy characteristics of materials, in particular, modern methods of molybdate production are used [6], as well as nanocomposites with carbon material are formed. This article presents the results of electrochemical studies of nanocrystalline nickel molybdates obtained by the hydrothermal method.

I. Materials and methods

In this work we have obtained nanocrystalline $NiMoO_4 \cdot H_2O$ by hydrothermal method according to the

O.M. Popovych, I. M. Budzulyak, O.V. Popovych, B.I. Rachiy, R.V. Ilnytskyi, L.S. Yablon, O.V. Morushko

procedure presented by the authors [5], namely 5.8 g of nickel nitrate (Ni(NO$_3$)$_2$·6H$_2$O) and 1.2 g of sodium molybdate (Na$_2$MoO$_4$·2H$_2$O) we dissolved in 40 ml of distilled water, stirring thoroughly. The solution was transferred to autoclave and kept in a furnace at 453 K for 2 hours. The autoclave was cooled at room temperature and then the resulting precipitate was washed several times in distilled water and dried in an air atmosphere in the furnace at a temperature of 343 K. The alpha phase of nickel molybdate (α-NiMoO$_4$) was obtained by annealing the hydrate at temperature of 673 K in an air atmosphere in the furnace for 2 hours.

Electrochemical studies in the three-electrode cell were performed on the 8-channel charge / discharge stand «Tionid» by galvanostatic and potentiodynamic methods. The working electrodes were formed from synthesized molybdates, the platinum electrode was the auxiliary, and the silver chloride electrode was the reference electrode. Aqueous solution of potassium hydroxide (33 %) was used as an electrolyte. The working electrode was formed from a mixture of 80 % nickel molybdate and 20 % conductive additive (acetylene carbon black), which was mixed with alcohol and pressed into a nickel mesh with an area of 25 mm^2. The mass of active material was approximately 15 mg in each electrode. Similarly, electrodes were formed for a hybrid supercapacitor (HSC), in which the obtained nickel molybdates were used as cathodes and activated carbon [7] was used as the anode.

II. Results and discussions

Cyclic voltammograms (CVs) of electrodes based on hydrothermally obtained nickel molybdates are presented in Fig. 1 a, b. The obtained CV curves are visually different from CV curves of pseudocapacitive materials such as MnO$_2$, RuO$_2$, which are characterized by almost rectangular shapes [8]. The accumulated charge during the electrochemical cycle can be divided into three components: faradaic charge from the process of ionic intercalation into the structure of the material, faradaic charge from redox reactions or pseudocapacitance, and

non-faradaic charge or the capacitance of the electric double layer (EDL).

Redox peaks on CVs are the result of the interaction of nickel ions from the structure of molybdate with hydroxyl ions from the electrolyte. This produces nickel hydroxide, which is converted into nickel oxyhydroxide according to the scheme shown in Fig. 2 and according to the following reactions [9]:

$$Ni^{2+} + 2OH^- = Ni(OH)_2$$

$$Ni(OH)_2 + OH^- = NiOOH + H_2O + e^-$$

From Fig. 1 a, b it is notably that the redox peaks of the electrodes based on hydrate and alpha nickel molybdate are asymmetric, which indicates the behavior of battery-type electrode. One reason for this behavior may be that the γ-NiOOH formed during the redox reaction has a layered structure. This structure provides space for K$^+$ ion intercalation, but thus reduces the reversibility of the molybdate structure.

We applied the empirical model proposed by J. Wang [10] to estimate the relative contribution of faradaic and non-faradaic processes to the total capacitance. The dependence of current on the scan rate was used to quantify the capacitive contribution to the current by the Cottrell equation: $i = \frac{nFAC_j^0\sqrt{D^0}}{\sqrt{\pi t}}$ (where i – current, n – number of electrons, F – Faraday's constant, A – electrode area, C_j^0 - the initial concentration of electrolyte ions, D^0 - diffusion coefficient, t – time) or in simplified form $i = at^{-1/2}$, where a – all constants. In addition, we can use scan rate $s^{1/2}$ instead of $t^{-1/2}$. Thus, the dependence of current on the scan rate is described by the power law $i = as^b$, where i – current, in A, s - scan rate, mV/s, a and b – adjustable parameters. From the dependences of $logi$ on $logs$, we can calculate the b-value which is equal to the slope of the approximating curve, since $logi = loga + blogs$. According to studies [11] for surface reactions $b = 1$ (processes not controlled by diffusion) and $i = as$, while for an ideal Faraday process controlled by diffusion $b = 0.5$ and the current is directly proportional to the square root of the scan rate: $i = a\sqrt{s}$.
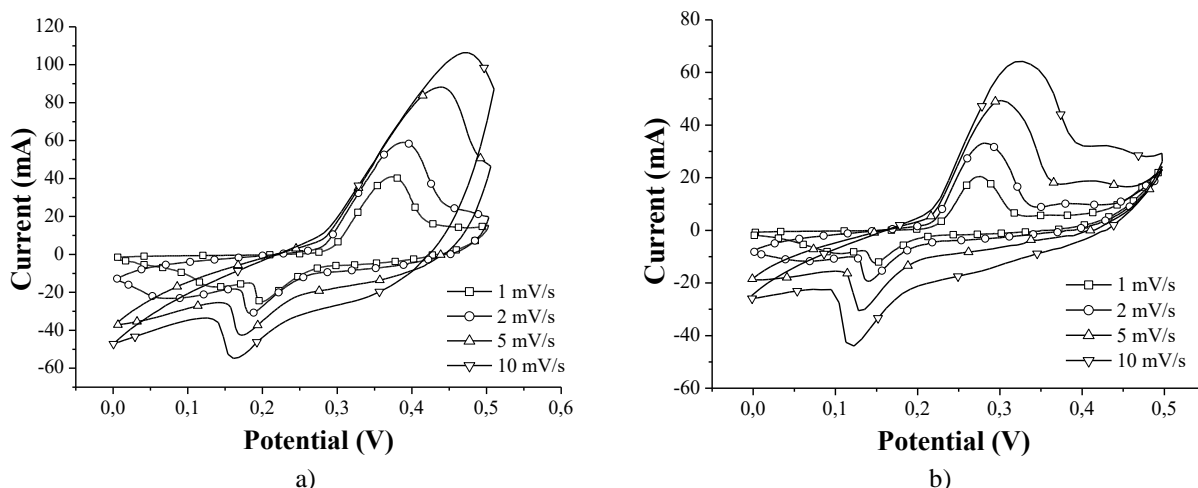

a)   b)

Fig. 1. CVs of (**a**) NiMoO$_4$·H$_2$O and (**b**) α-NiMoO$_4$ electrodes at a various scan rates from 1 to 10 mV/s.
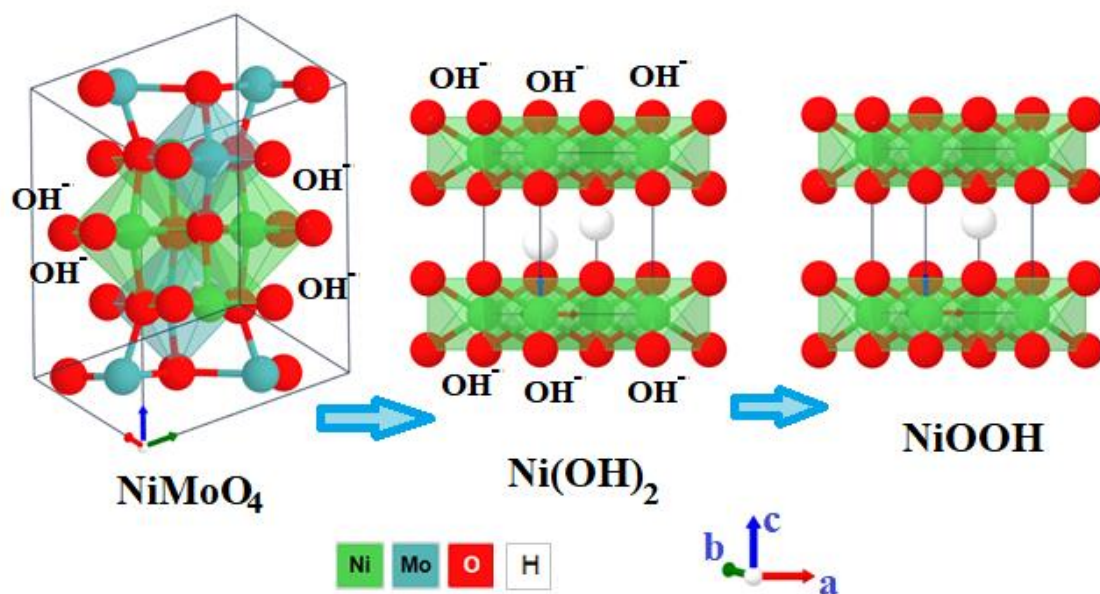
Fig.2. Schematic representation of the process of electrochemical reaction of nickel molybdate electrodes.
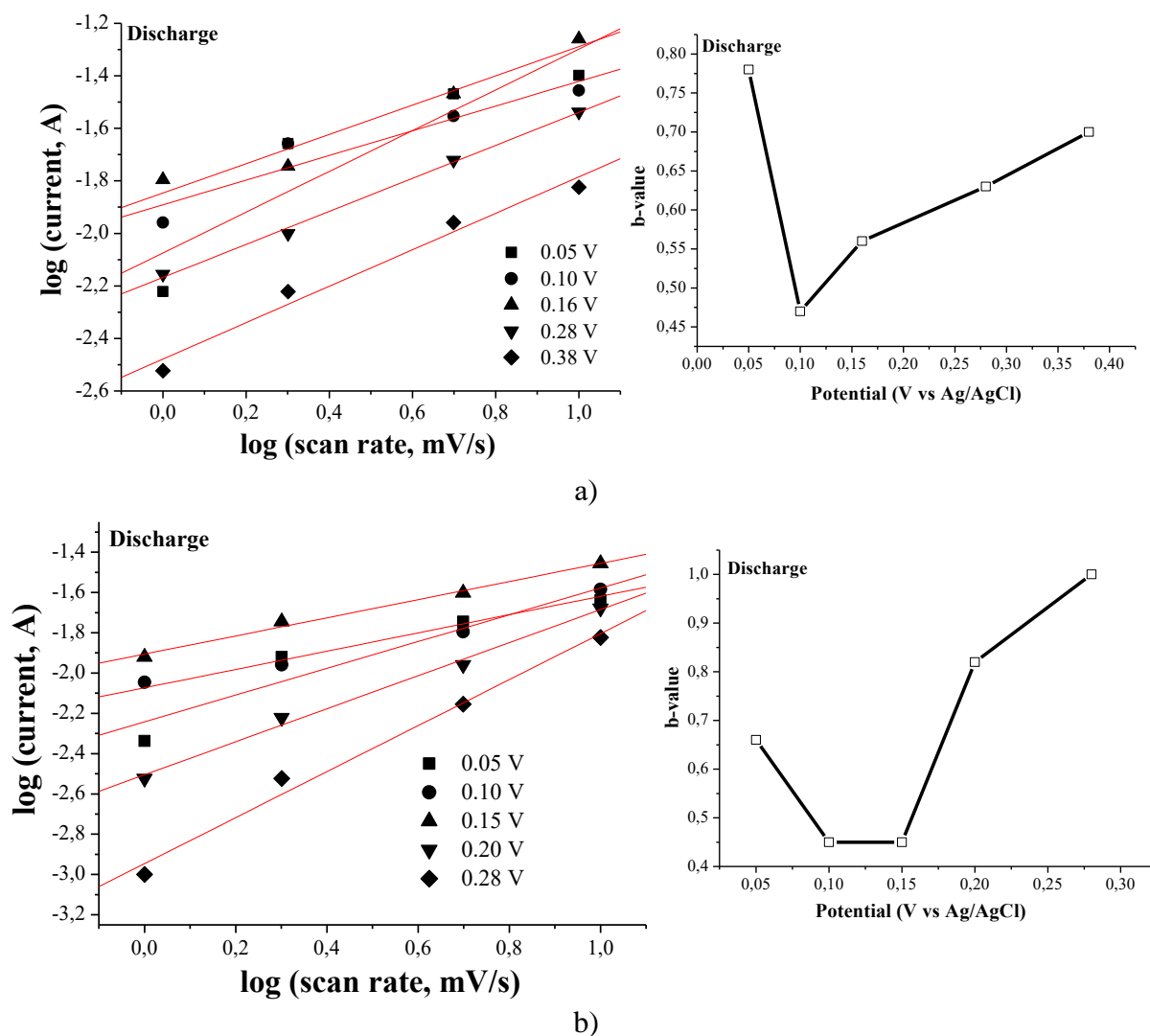

a)

b)

Fig.3. The plots of *log i* vs. *log s* derived from discharge CVs and the dependence of the slope b as a function of cell voltage for (**a**) $NiMoO_4 \cdot H_2O$ and (**b**) α-$NiMoO_4$ electrodes

O.M. Popovych, I. M. Budzulyak, O.V. Popovych, B.I. Rachiy, R.V. Ilnytskyi, L.S. Yablon, O.V. Morushko

The logarithmic dependences of currents on the scan rate at discharge and fixed potential values for the NiMoO$_4$·H$_2$O and α-NiMoO$_4$ electrodes and the corresponding *b*-values are presented in Fig. 3 a, b.

The *b*-value is relatively low at the redox peaks potentials, its indicates the dominance of diffusion-controlled intercalation of electrolyte ions, while at potentials lower and higher than the potentials of peak formation, the *b*-values are in the range of 0.7 - 1.0 V, which indicates capacitive mechanism of charge accumulation. Thus, the current in this potential range is the sum of the two contributions arising from the redox pseudocapacitance plus EDL capacitance and intercalation:

$$i(U)=k_1 s + k_2 s^{1/2} \quad \text{or} \quad i(U)/s^{1/2}=k_1 s^{1/2} + k_2,$$

where $k_1 s$ and $k_2 s^{1/2}$ correspond to surface capacitive effects and diffusion-controlled intercalation process respectively. To determine the k_1 and k_2 coefficients it is necessary to obtain the dependence of $i(U)/s^{1/2}$ on $s^{1/2}$, the slope of the line will be equal to k_1, while its intersection with the y-axis – k_2. The plots of $i/s^{1/2}$ on $s^{1/2}$, which were used to calculate the k_1 and k_2 values at different potentials and scan rates from 1 to 10 mV/s and subsequent calculation of the percentage of bulk and

surface reactions are presented in Fig. 4.

Therefore, the contribution from surface and bulk electrochemical reactions at the lowest scan rate in the hydrate-based electrode is 14 % and 86 %, respectively, and for α-NiMoO$_4$ – 29 % and 71 %. Also from the diagrams it is noticeable that with increasing scan rate up to 10 mV/s the percentage of charge accumulated as a result of surface pseudocapacitance and EDL capacitance increases to 32 % for NiMoO$_4$·H$_2$O and to 44 % for α-NiMoO$_4$ due to the fast charge / discharge time.

Dependence of specific capacitances on the scan rate calculated from cyclic voltammograms according to: $C = \frac{Q}{m\Delta U}$, where Q - the charge is given (accumulated) by the electrochemical system during cathode (anode) scanning, m - mass of material, ΔU - range of potentials, is presented in Fig. 5. Hydrate nickel molybdate shows the highest specific capacitance of 621 F / g at a scan rate of 1 mV / s in the potential range of 0 - 0.5 V, while for α-NiMoO$_4$ the maximum capacitance is 281 F/g. The redox processes are not related to molybdenum atoms because its oxidation state is +6 and it doesn't undergo transformations upon OH$^-$ ion intercalation. In the case of cathode potential scanning, Mo does not undergo the reduction process due to the limited potential window, which agrees well with the data for the
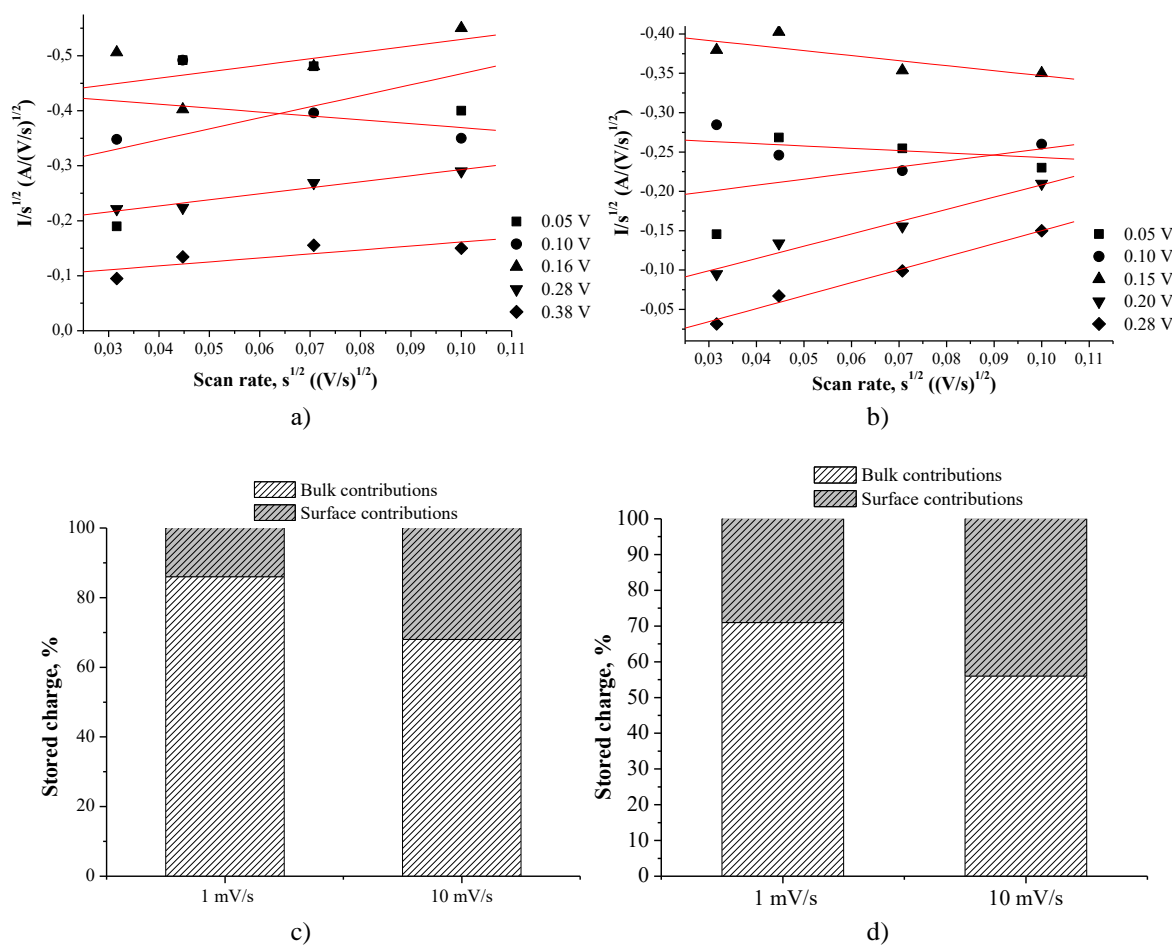
Fig. 4. The plots of $I/s^{1/2}$ vs. $s^{1/2}$ used to calculate the constants k_1 and k_2 at different potentials with scan rates varied from 1–10 mV/s for (**a**) NiMoO$_4$·H$_2$O and (**b**) α-NiMoO$_4$ electrodes. Bar chart showing the percentage contribution of stored charge from surface reaction and bulk reaction as a function of scan rate for (**c**) NiMoO$_4$·H$_2$O and (**d**) α-NiMoO$_4$ electrodes.

MnMoO$_4$/CoMoO$_4$ electrode material [12], where the pseudocapacitance arises from the Faraday redox reactions of Mn and Co, but Mo does not participate in them. Confirmation that molybdenum atoms improve the electrical conductive properties of the material is a study [13] in which nickel hydroxide modified by ultrasonic dispersion reached a specific capacitance of 341 F/g at 1 mV/s, while pure β-nickel hydroxide only 238 F/g [14] which is less than the results obtained in this study. Therefore, the main function of molybdenum atoms in the material is to increase the electrical conductivity of molybdate and thus improve the electrochemical properties of the system.

The specific capacitances of both samples decrease significantly with increasing scan rate. Faradaic reactions occurring on the surface of materials can be rewritten as follows [15]:

$$NiMoO_4 + yOH^- + e^- \leftrightarrow NiMoO_{4-y} \cdot yOH^- +$$
$$+(1-y) NiMoO_4 + H_2O + e^-,$$
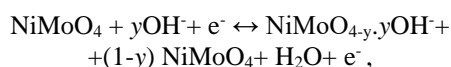
where y represents the total number of active centers on the surface of amorphous nickel molybdate. The above reaction shows that only part of the active centers involved in the redox reaction (when $y = 1$ all plots are involved). The value of y for all systems was calculated using the following equation:
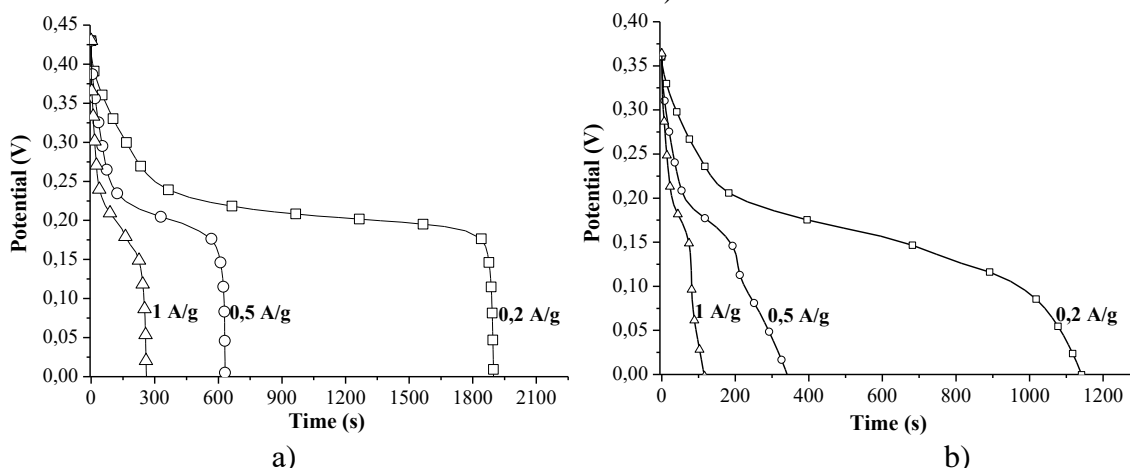
$$y = \frac{CM\Delta U}{F},$$

where C is the specific capacitance (F/g), M - molecular weight of active element (nickel) (58.6 g/mol), ΔU – range of potentials, F - Faraday's constant (96500 C/mol). The value of y is equal to 0.2 for NiMoO$_4$·H$_2$O and 0.09 for α-NiMoO$_4$ at a scan rate of 1 mV/s, which means ~ 2.5 times more active centers than at 10 mV/s (y = 0,08 for NiMoO$_4$·H$_2$O and y = 0,04 for α-NiMoO$_4$). The decrease in the specific capacitance with increasing scan rate can be explained by the limited flow of ions into the internal structure of the electrode and the passage of only rapid surface reactions, which agrees well with the data presented in the Fig. 4 c, d.

The coulombic efficiency for the hydrate-based electrode is 95 % and doesn't change after 100 cycles, while for α-NiMoO$_4$ it reaches a maximum of 65 % and gradually decreases with increasing cycle number (Fig. 5, b). The specific capacitance is 40% of the initial capacitance for both NiMoO$_4$·H$_2$O and for α-NiMoO$_4$ electrodes after 100 cycles.

Galvanostatic discharge curves are presented in Fig. 6, their nonlinearity indicates the redox behavior of the studied materials, which is confirmed by CV data.

a)

b)
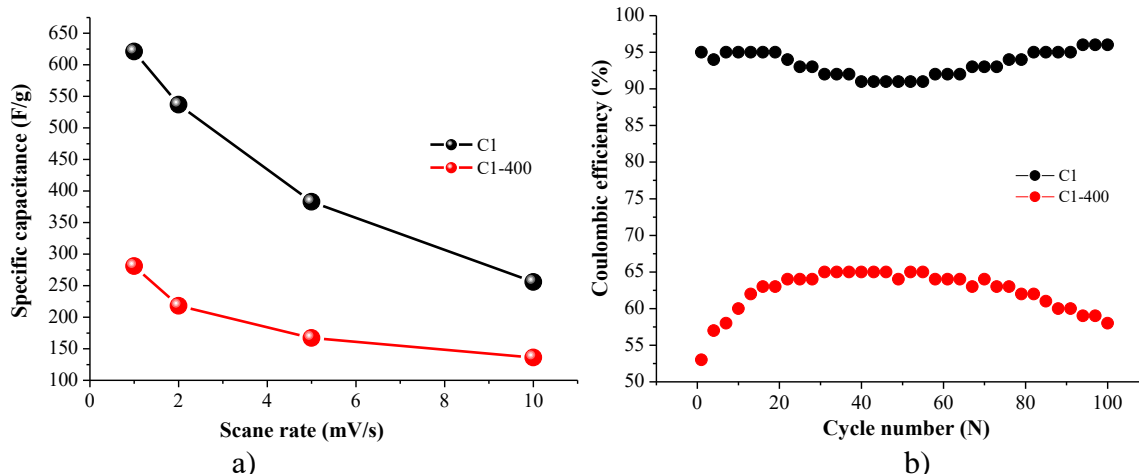
Рис.5. (*a*) Discharge specific capacitances vs. scan rates and (*b*) coulombic efficiency vs. number of cycles for electrodes based on NiMoO$_4$ · H$_2$O (sample C1) and α-NiMoO$_4$ (sample C1-400)


a)

b)

Fig.6. Galvanostatic discharge curves of (a) NiMoO$_4$ · H$_2$O and (b) α-NiMoO$_4$ electrodes

O.M. Popovych, I. M. Budzulyak, O.V. Popovych, B.I. Rachiy, R.V. Ilnytskyi, L.S. Yablon, O.V. Morushko

Table 1.

Specific capacitances calculated from cyclic voltammograms and galvanostatic discharge curves

| Method	Cyclic voltammetry				Galvanostatic Method		
	Scan rate, mV/s				Current, A/g		
	1	2	5	10	0,2	0,5	1
NiMoO$_4$ · H$_2$O	621	537	383	256	882	734	604
α-NiMoO$_4$	281	218	167	136	633	475	322

a)

b)

c)
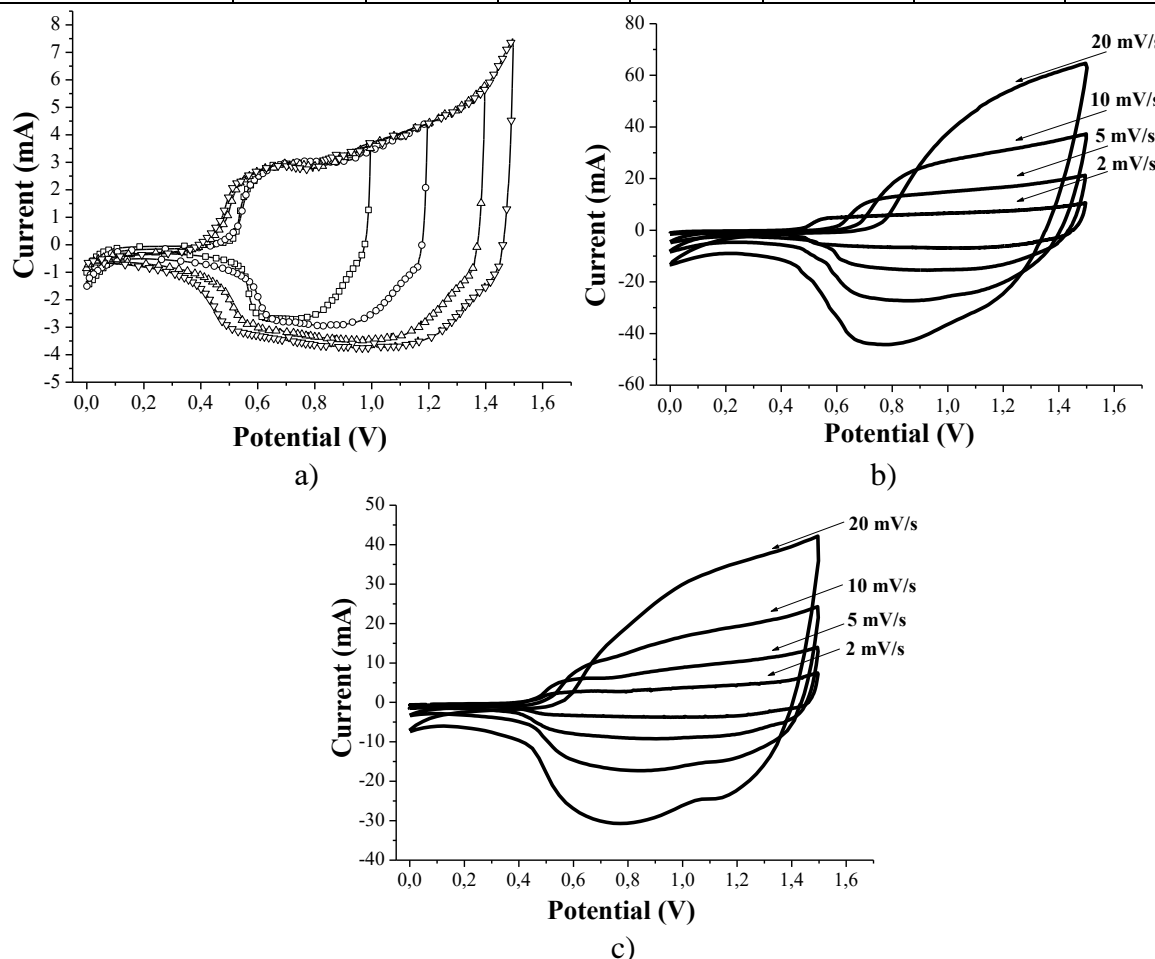
Fig.7. (*a*) Determination of the operating potential range of hybrid supercapacitor α-NiMoO$_4$ / C at scan rate 2 mV/s.
CVs of HSCs (*b*) NiMoO$_4$ · H$_2$O / C and (*c*) α-NiMoO$_4$ /C

Table 1 represents the values of specific capacitances calculated from cyclic voltammograms and galvanostatic discharge curves ($C = \frac{I \Delta t}{m \Delta U}$, I – current, Δt – discharge time). NiMoO$_4$·H$_2$O electrode has the largest specific capacitance of 882 F/g at a discharge current of 0.2 A/g. This can be explained by the fact that the amorphous nature of the electrode material promotes better diffusion-controlled reactions and, accordingly, the use of a larger volume of material.

We have formed hybrid two-electrode cells to determine the practical application of electrodes based on nickel molybdates. The selection of the operating potential range of hybrid supercapacitors was carried out by cyclic voltammetry. It was found that the operating range of HSCs is 0 - 1.5 V (Fig. 7 a). Wider potential operating range allows increasing specific energy in comparison with EDL supercapacitors. CV curves of HSCs NiMoO$_4$·H$_2$O/C and α-NiMoO$_4$/C at scan rates of 2, 5, 10 and 20 mV/s are represented in Fig. 7, b, c. Hybrid supercapacitors in this potential range demonstrate quasi-rectangular shapes of cyclic voltammograms. As the scan rate increases, the shape of the CV curves almost unchanged.

Galvanostatic charge / discharge tests of HSCs performed at specific currents of 0.2, 0.5 and 1 A/g are represented in Fig. 8. The nonlinearity of the curves confirms the pseudocapacitive behavior of the cathode material caused by electrochemical adsorption and redox
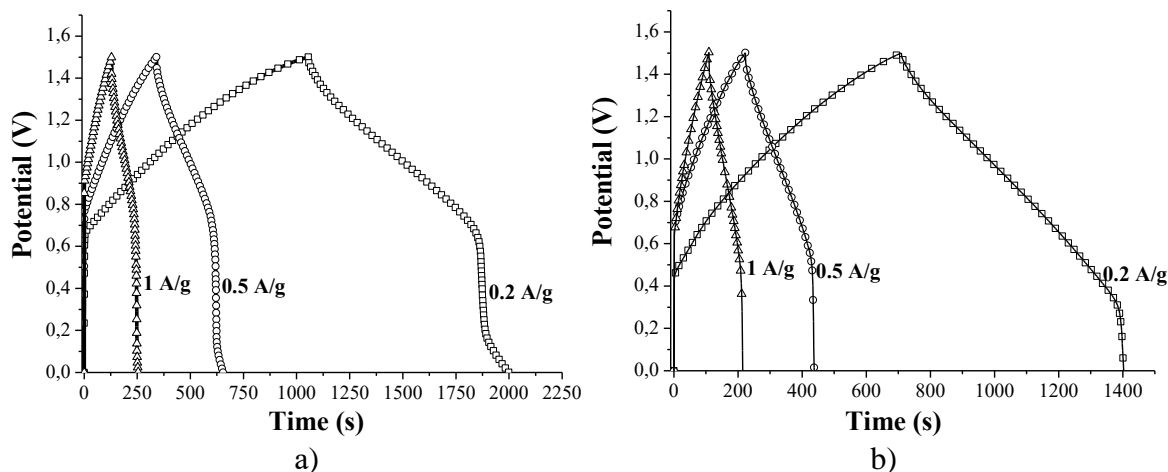
Fig.8. Galvanostatic charge / discharge curves of HSCs (a) $NiMoO_4 \cdot H_2O$ / C and (b) α-$NiMoO_4$ / C
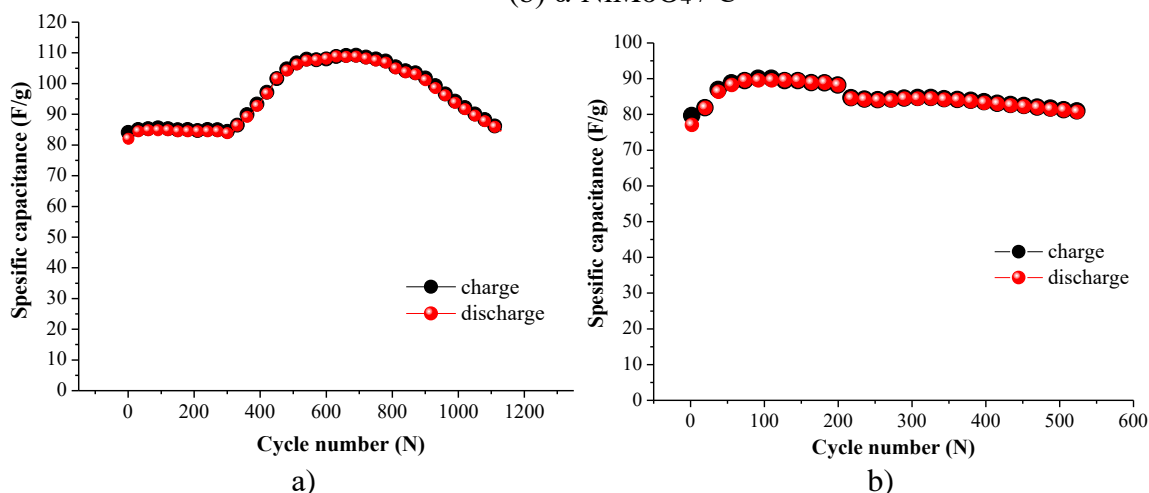
Fig.9. Discharge specific capacitances vs. number of cycles for electrodes based on (a) $NiMoO_4 \cdot H_2O$ and (b) α-$NiMoO_4$ at current 1 A/g

reactions at the electrode / electrolyte interface. The specific capacitance of HSC based on $NiMoO_4 \cdot H_2O$ was 256, 215 and 176 F/g at currents of 0.2, 0.5 and 1 A/g respectively. The specific capacitance of HSC based on α-$NiMoO_4$ was 188, 151 and 148 F/g at currents of 0.2, 0.5 and 1 A/g respectively. We also calculated the specific energy and power of HSCs, which were 80 W h/kg and 304 W/kg for $NiMoO_4 \cdot H_2O$/C and 59 W h/kg, 304 W/kg for α-$NiMoO_4$/C.

The cyclic stability of hybrid supercapacitors was investigated by charge / discharge testing for 500 or more cycles at a current of 1 A/g. The dependences of the specific capacitance of the HSC on the cycle number are represented in Fig. 9. The specific capacitance of HSC $NiMoO_4 \cdot H_2O$/C in the initial 300 cycles is almost unchanged. Over the next 300 cycles the specific capacitance increases and reaches a maximum value of 110 F/g, then decreases linearly. For HSC based on α-$NiMoO_4$ / C there is an increase in specific capacitance in the first 100 cycles to 90 F/g, followed by a linear decrease in subsequent cycles. The coulombic efficiency of the studied HSCs is 99.5 % and is maintained throughout the charge / discharge cycle. This behavior of hybrid supercapacitors can be caused by degradation of the structure of materials due to redox reactions,

agglomeration of particles and changes in the internal volume of the structure of molybdates, as well as due to the aging of supercapacitors. Although the specific capacitance drop is present in both HSCs, reducing the capacitance drop rate with more cycles improves the possibility of long-term cyclic stability of the $NiMoO_4 \cdot H_2O$ electrode and, consequently, its practical application in energy-storage devices.

Conclusions

In this paper, the contribution of surface and bulk processes to the total capacitance of the studied materials is estimated. It was found that nanocrystalline $NiMoO_4 \cdot H_2O$ has a maximum specific capacitance of 621 F/g at a scan rate of 1 mV/s. This capacitance is provided by the charge accumulated due to the intercalation of electrolyte ions into the structure of molybdate (86 %) and also by redox reactions and EDL capacitance (14 %). For α-$NiMoO_4$ there is a decrease in specific capacitance to 281 F/g, but the content of the capacitive mechanism of charge accumulation increases to 29 %. Nanocrystalline nickel molybdate hydrate provides more surface-active centers for redox reactions

O.M. Popovych, I. M. Budzulyak, O.V. Popovych, B.I. Rachiy, R.V. Ilnytskyi, L.S. Yablon, O.V. Morushko

and promotes sufficient access of electrolyte ions in the internal structure of the material. This together provides higher electrochemical characteristics compared to the α-phase, namely longer cyclic stability, higher specific energy and specific capacitance of the hybrid supercapacitor based on hydrate.

Acknowledgment

Popovych O.M. - Doctoral student;
Budzulyak I.M. - Professor, Doctor of Physical and Mathematical Sciences;
Popovych O.V. – PhD student;
Rachiy B.I. – Professor, Doctor of Physical and Mathematical Sciences;
Ilnytskyi R.V. – Professor, Doctor of Physical and Mathematical Sciences;
Yablon L.S. - Professor, Doctor of Physical and Mathematical Sciences;
Morushko O.V. – PhD, head of the laboratory.

[1] O.M. Khemii, I.M. Budzuliak, V.O. Kotsyubynsky, L.S. Yablon, R.V. Ilnytskyi, V.M. Boychuk, O.V. Morushko, K.V. Bandura, M.M. Khemii, Materials Science-Poland 37(4), 547 (2019) (DOI: https://doi.org/10.2478/msp-2019-0077).

[2] R.N. Singh, J.P. Singh, A. Singh, Int. J. Hydrogen Energy 33(16), 4260 (2008) (DOI: https://doi.org/10.1016/j.ijhydene.2008.06.008).

[3] K. Eda, Y. Kato, Y. Ohshiro, T. Sugitani, & M. S. Whittingham, Journal of Solid State Chemistry 183(6), 1334 (2010) (DOI: https://doi.org/10.1016/j.jssc.2010.04.009).

[4] J.A. Rodriguez, S. Chaturvedi, J.C. Hanson, A. Albornoz, J.L. Brito, J. Phys. Chem. B 102(8), 1347 (1998) (DOI: https://doi.org/10.1021/jp972137q).

[5] B. Senthilkumar, R.K. Selvan, Journal of colloid and interface science 426, 280 (2014) (DOI: https://doi.org/10.1016/j.jcis.2014.04.010).

[6] O.M. Popovych, I.M. Budzulyak, V.O. Kotsyubynsky, O.V. Popovych, B.I. Rachiy, R.V. Ilnytskyi, L.S. Yablon, Physics and Chemistry of Solid State 21(4), 650 (2020). (DOI: https://doi.org/10.15330/pcss.21.4.650-659).

[7] B.I. Rachiy, I.M. Budzulyak, V.M. Vashchynsky, N.Y. Ivanichok, M.O. Nykoliuk, Nanoscale Research Letters 11(1), 18 (2016) (DOI: https://doi.org/10.1186/s11671-016-1241-z).

[8] G.Z. Chen, International Materials Reviews 62(4), 173 (2017) (DOI: https://doi.org/10.1080/09506608.2016.1240914).

[9] S.W. Zhang, B.S. Yin, C. Liu, Z.B. Wang, & D.M. Gu, Applied Surface Science 458, 478 (2018) (DOI: https://doi.org/10.1016/j.apsusc.2018.07.110).

[10] J. Wang, J. Polleux, J. Lim, B. Dunn, J. Phys. Chem. C. 111(40), 14925 (2007) (DOI: https://doi.org/10.1021/jp074464w).

[11] V. Augustyn, P. Simon, B. Dunn, Energ Environ. Sci. 7(5) 1597 (2014) (DOI: https://doi.org/10.1039/C3EE44164D).

[12] L.Q. Mai, F. Yang, Y.L. Zhao, X. Xu, L. Xu, Y.Z. Luo, Nat. Commun. 2, 381 (2011) (DOI: https://doi.org/10.1038/ncomms1387).

[13] I.M. Budzulyak, O.M. Khemii, O.V. Morushko, D.I. Popovych, Yu. Starchuk, L.S. Yablon, Nanosistemi, Nanomateriali, Nanotehnologii 17(4), 0689 (2019) (DOI: https://www.imp.kiev.ua/nanosys/media/pdf/2019/4/nano_vol17_iss4_p0689p0700_2019.pdf).

[14] O.M. Hemiy, L.S. Yablon, I.M. Budzulyak, S.I. Budzulyak, O.V. Morushko, A.I. Kachmar, J. Nano- Electron. Phys. 8 (4), 04074 (2016) (DOI: https://doi.org/10.21272/jnep.8(4(2)).04074).

[15] R. Ranjusha, S. Ramakrishna, A.S. Nair; P. Anjali, S. Vineeth, T.S. Sonia, B N. Sivakumar, K.R.V. Subramanian, S.V. Nair, A. Balakrishnan, RSC Adv. 3, 17492 (2013) (DOI: https://doi.org/10.1039/C3RA41992D).

Synthesis and Electrochemical Properties of Nanocrystalline Nickel Molybdate

О.М. Попович, І. М. Будзуляк, О.В. Попович, Б.І. Рачій, Р.В. Ільницький, Л.С. Яблонь, О.В. Морушко

Синтез та електрохімічні властивості нанокристалічного молібдату нікелю

Прикарпатський національний університет ім.В.Стефаника, Івано-Франківськ, Україна, khemiiolha@gmail.com

В роботі отримали нанокристалічний молібдат нікелю гідратований та альфа-фазу гідротермальним методом. На основі аналізу даних циклічної вольтамперометрії нами оцінено внесок фарадеївських та нефарадеївських процесів в загальну ємність досліджуваних молібдатів. Встановили, що максимальної питомої ємності 621 Ф/г при швидкості сканування 1 мВ/с досягає гідратований $NiMoO_4 \cdot H_2O$, в той час як питома ємність $\alpha\text{-}NiMoO_4$ становить 281 Ф/г. На основі синтезованих молібдатів нікелю сформовані катоди для гібридних суперконденсаторів. В результаті проведених електрохімічних досліджень встановлено, що питома ємність гібридного суперконденсатора на основі $NiMoO_4 \cdot H_2O/C$ становила 256 Ф/г при струмі 0,2 А/г, тоді як питома енергія та потужність – 80 Вт год/кг і 304 Вт/кг і ці результати є вищі, ніж гібридного суперконденсатора на основі $\alpha\text{-}NiMoO_4/C$.

Ключові слова: молібдат нікелю, гідрат, циклічна вольтамперограма, питома ємність, кулонівська ефективність, активований вуглець, гібридний суперконденсатор.